ARTICLE OPEN

Check for updates

Accelerating corrosion inhibitor discovery through computational routes: a case of naphthalene 1-thiocarboxamide

Dharmendr Kumar[1]✉, Venkata Muralidhar K[1], Vinay Jain[1] and Beena Rai[1]

The conventional approach to the discovery of corrosion inhibitors is time-consuming and requires a significant amount of resources. In the present study, we highlight the use of a first principles DFT-based approach to expedite the rational design and discovery of corrosion inhibitors for mild steel in acidic media. From among various sulfur containing molecules shortlisted based on quantum chemical descriptors, naphthalene 1-thiocarboxamide (NTC) is found to have the lowest E_{LUMO} and E_{gap}, suggesting best corrosion inhibition. Subsequently, explicit adsorption studies reveal strong chemisorption of NTC onto the Fe (001) surface, characterized by a plethora of Fe-C/N/S covalent bonds. DFT Surface coverage studies additionally indicate the formation of a compact monolayer of NTC on the Fe surface. Gravimetric, potentiodynamic polarization, and Electrochemical Impedance Spectroscopy studies, all confirm NTC as a remarkable inhibitor for mild steel in 1 N HCl at both room and elevated (60 °C) temperatures even at merely 1 mM concentration.

npj Materials Degradation (2024)8:5 ; https://doi.org/10.1038/s41529-023-00421-x

INTRODUCTION

Corrosion inhibitors (CI's) play a critical role in combating corrosion in various industrial applications[1]. For example, the oil and gas industry extensively uses CI's for well acidizing wherein strong, corrosive acids such as HCl and/or HF are pumped through steel tubings and casings at high temperatures and pressures in order to enhance the permeability of the rocks and, thus, increase productivity[2–5]. Owing to increasingly stringent environmental norms and increasing depths of oil and gas wells, there is a need for design of newer and more efficient CI's. However, the conventional CI design and discovery is a largely empirical, cost and time-intensive process, characterized by hundreds of trial-and-error experiments. Sometimes, it may cost millions of dollars and several years to come up with a single new CI molecule for a particular application. For instance, Meier and Xie[6] indicate that it took them almost 4 years, and development & screening of more than 400 individual molecules to come up with a single new inhibitor molecule for copper corrosion inhibition in cooling water applications in the presence of halogen based oxidizing biocides (such as HOCl and HOBr).

Although, computational techniques (such as molecular modeling/ machine learning) have been in vogue for the last couple of decades, their use has been largely confined to predicting inhibition mechanisms of known CI's rather than discovery of new CI molecules per se barring a few works especially by Winkler et al.[7–10]. In this paper, we highlight the use of first principles density functional theory (DFT) based approaches (Fig. 1) in order to expedite rational CI design and discovery (and thus, complement experiments). Specifically, our work elucidates the DFT-based discovery of naphthalene 1-thiocarboxamide (NTC) as an excellent CI for steels at both room as well as elevated temperatures (60 °C) in HCl environment. We have performed detailed DFT-based quantum chemical, adsorption and coverage studies followed by experimental gravimetric and electrochemical studies to conclusively establish our findings.

RESULTS AND DISCUSSION

Quantum chemical descriptors

Quantum chemical descriptors (QCDs) were calculated from the NWchem optimized geometries. QCDs such as the highest occupied molecular orbital (E_{HOMO}), lowest unoccupied molecular orbital (E_{LUMO}) and E_{gap} (E_{LUMO}- E_{HOMO}) are important parameters to explain the reactivity of a molecule. HOMO and LUMO (Fig. 2) can be seen to be spread throughout the NTC molecule suggesting a flat orientation on the Fe surface to be more stable. E_{HOMO} generally indicates the capacity of the molecule to donate electrons while E_{LUMO} indicates its capacity to accept electrons[11]. As reported in literature, molecules having high E_{HOMO} and low E_{LUMO} (both close to metal E_{Fermi}) are generally considered to be good CI's as these would allow easy flow of electrons from molecule to metal (E_{HOMO}) and vice-versa (E_{LUMO})[12]. Similarly, lower E_{gap} generally corresponds to better reactivity of the molecule[13]. The more reactive molecules are likely to adsorb on the metal surface to form a protective layer, which in turn prohibits the direct contact of the metal surface with corrosive elements.

In our efforts to identify suitable CI's for vapor phase corrosion inhibition (VCI), we tried to compare the E_{gap} values for a few, hitherto untested, sulfur containing compounds with that of 11-mercaptoundecanoic acid—a known VCI for steels[14]. Among the list of molecules tried, we found NTC to show the lowest E_{gap} (Table 1) and therefore, potentially, the best inhibition efficiency. Obviously, this list is not exhaustive, and there can be certainly many more S-compounds with potential as inhibitors. However, for practical purposes, we limited ourselves to these molecules.

Adsorption studies

QCDs may serve as a good screening aid for identifying potential inhibitor molecules. However, being metal surface agnostic, they may not always work for all metals; moreover, they do not provide

[1]Physical Sciences Research Area, TCS Research, Sahyadri Park 2, Rajiv Gandhi Infotech Park, Hinjewadi - Phase 3, Pune, Maharashtra, India. ✉email: dharmendr.9@tcs.com

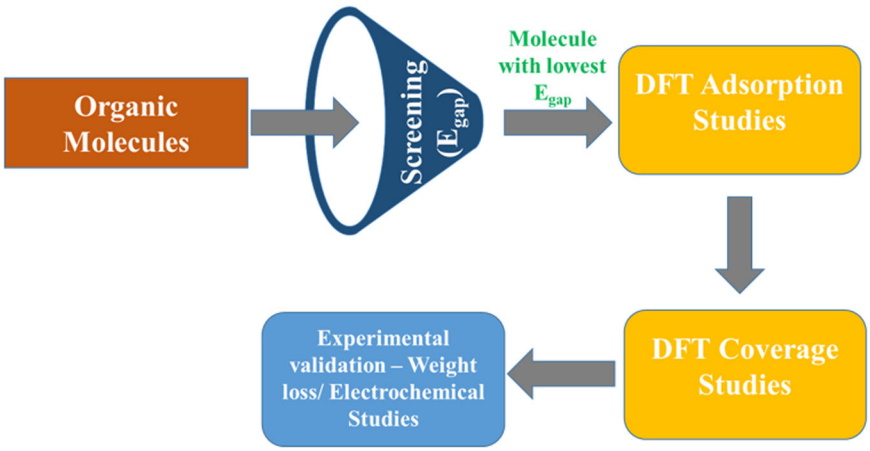

Fig. 1 Framework for rational screening/ design of new organic CI's. E_{gap} refers to HOMO-LUMO gap calculated using DFT.

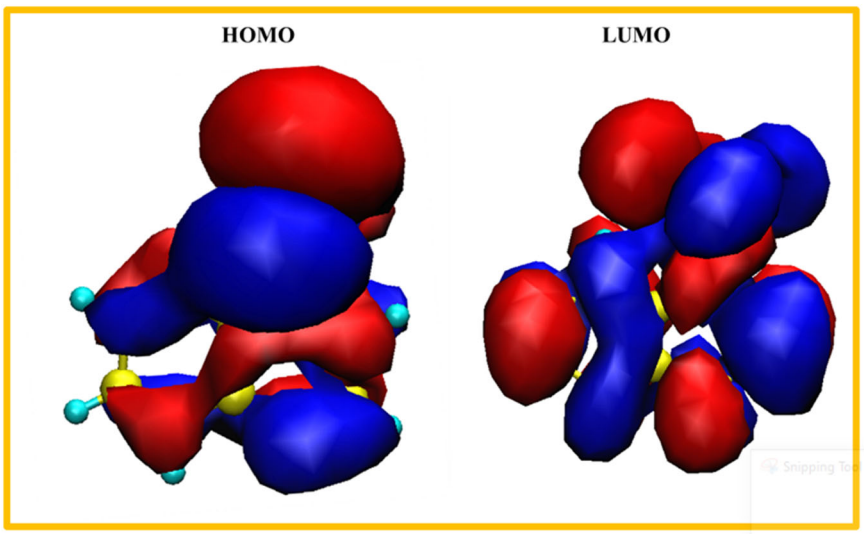

Fig. 2 HOMO, LUMO plots of NTC molecule. Isovalue: ± 0.08 eV Å^−3.

Table 1. E_{HOMO}, E_{LUMO} and E_{gap} of various sulfur containing compounds.

S. No.	Molecule	E_{HOMO} (eV)	E_{LUMO} (eV)	E_{gap} (eV)
1	Naphthalene-1-thiocarboxamide	−5.89	−1.85	4.04
2	Dimethyl disulfide	−5.63	−1.4	4.23
3	1,2,4 – Trithiolane	−6.48	−1.69	4.79
4	Propyl propanethiosulfonate	−7.24	−1.59	5.65
5	Bis(methyl)thiomethane	−6.26	−0.43	5.84
6	11-Mercaptoundecanoic acid	−6.57	−0.72	5.85
7	Allyl isothiocyanate	−6.88	−0.98	5.91
8	Dimethyl sulfoxide	−6.49	−0.47	6.02
9	3-Mercapto-2-methylpentan-1-ol	−6.63	−0.39	6.24

insight into the underlying inhibition mechanisms[15]. Therefore, explicit adsorption studies become imperative to further probe and establish the nature and strength of the molecule-metal surface interactions.

Several conformations (conf1-4) of NTC were considered on Fe (001) surface in order to arrive at the most stable adsorption geometry. The initial and optimized adsorption geometries are shown in Fig. 3 while the corresponding ΔE_{ads} are shown in Fig. 4. It can be seen that the flat conformations strongly adsorb on Fe surface via Fe—C, Fe—N and Fe—S chemical bonds while vertical conformations adsorb via only Fe—S bonds. The average bond lengths of Fe—C, Fe—N and Fe—S are 2.16, 2.18 and 2.25 Å respectively. These bond lengths are close to the sum of the covalent radii of respective bond-forming atoms ($r_c^{Fe} + r_c^{C} = 1.32 + 0.76 = 2.08$ Å; $r_c^{Fe} + r_c^{N} = 1.32 + 0.71 = 2.03$ Å; $r_c^{Fe} + r_c^{S} = 1.32 + 1.05 = 2.37$ Å) suggesting that the bonds are of covalent type. Despite having similar initial conformations, conf1 and conf2 lead to significantly different final conformations and ΔE_{ads} values. On the other hand, conf3 and conf4 exhibit similar optimized adsorption geometries and ΔE_{ads} values; however, these ΔE_{ads} values are almost half that of the flat geometries (conf1 and conf2).

Clearly, the flat orientation of the molecule in Conf1 facilitates extensive interactions between practically all the atoms of the NTC molecule and the underlying surface Fe atoms. In fact, a comparison of the $|\Delta E_{ads}|$ (= 4.54 eV) values for NTC with that of another commonly used inhibitor, *trans*-cinnamaldehyde (TCA) ($|\Delta E_{ads}|$ = 3.89 eV), reported in our earlier publication[16] suggests

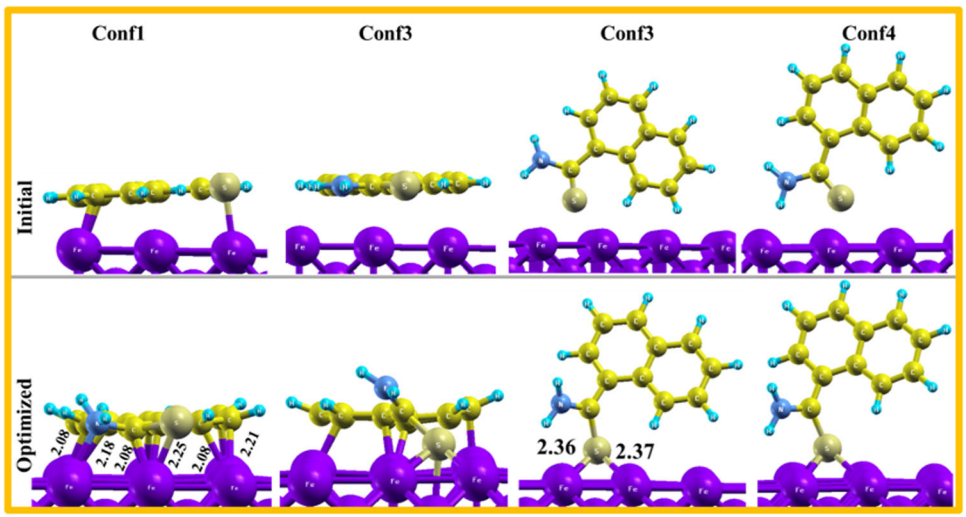

Fig. 3 Initial and optimized adsorption geometries of NTC on Fe surface. Violet, Yellow, Pale Yellow, Blue and Aqua represent Fe, C, S, N, and H atoms respectively.

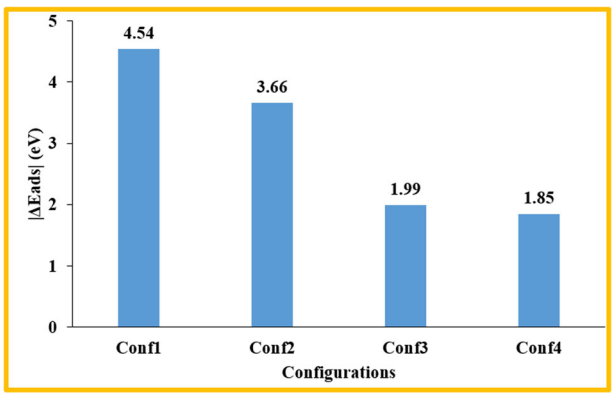

Fig. 4 Adsorption energies of different configurations of NTC adsorbed on Fe surface. Conf1 with flat orientation shows the highest magnitude of adsorption energy ($|\Delta E_{ads}|$).

that the former adsorbs much stronger (~17%) and, therefore, can be a promising inhibitor for steels.

Further, to shed some light on the interaction mechanism of NTC with Fe surface, electron density difference (EDD) and projected density of states (PDOS) were plotted for the most stable adsorption geometry (conf1). In the EDD plot (Fig. 5-Upper panel), blue regions show electron depletion while reddish-brown regions show electron accumulation. It is evident from the EDD plot that there is a significant charge redistribution happening between the molecule and the Fe surface because of strong hybridization of Fe-3d orbitals with C/N/S-2p orbitals. Moreover, the charge accumulation is occurring between C/N/S atoms of molecule and Fe atoms of the surface, thus, signifying that the bond formed between F—C/N/S is of covalent type[17]. The large perturbation of the electronic structure due to adsorption of NTC on Fe (001) also induces the sp^2 to sp^3 rehybridization of the molecular electronic structure—indicated by the shifting of H-atoms above the plane of the aromatic rings[18].

Lower panel of Fig. 5 shows the PDOS of C/N/S-atoms adsorbed on Fe surface. For isolated or unadsorbed molecule, the molecular peaks are quite sharp and discrete.However, post adsorption, the molecular peaks broaden and become continuous. Furthermore, it can also be seen that there are significantly higher number of overlapping peaks in Fe—S and it goes on decreasing from S to C to N. Thus, it can be concluded that the interaction between Fe—S is the strongest while Fe—N is the weakest among the three bonds.

The Bader charges (Table 2) were calculated using projector-augmented-wave (PAW) potentials and a charge density kinetic energy cutoff of 800 Ry, for the most stable optimized configuration (conf1, DFT-D3), employing the algorithm developed by Henkelman's group[19]. Analysis of Table 2 revealed a net transfer of charge ($\Delta = 1.74$ e) from the Fe surface to the NTC molecule. Notably, the S atom of NTC receives the highest amount of charge (−0.193e), while the C atoms receive −0.135e charge on an average. This suggests that S/C atoms play a significant role in the strong NTC-Fe interactions validating the PDOS results above.

Coverage studies

In addition to adsorption, corrosion inhibition also involves the creation of a compact, protective layer. The molecules must strongly adhere to the surface at high coverage to promote the formation of a protective film[20]. Therefore, it is essential to model coverage effects for a given CI molecule using DFT[16,21]. For this purpose, we have carried out detailed surface coverage studies for NTC on Fe (001) surface. The optimized structures for different coverages, viz. 1/48, 2/48, 3/48, and 4/48 in ML (where monolayer, ML, is the ratio of the number of inhibitor molecules to the number of metal atoms in the first layer of the surface) are displayed in Fig. 6. As shown in Fig. 7, the ΔE_{ads} decreases only slightly (~0.2 eV, 4.4%) with increase in coverage implying weak lateral repulsions between the molecules and therefore, formation of a more compact layer under actual conditions.

Apart from ΔE_{ads} computations at different coverages, we have also computed the adsorption surface free energy, γ_{ads}, which is the ΔE_{ads} normalized to a unit surface area and plotted as a function of the molecular chemical potential μ. This is done because as per Kokalj[22], γ_{ads} as a function of μ is a better indicator of stability. The γ_{ads} is given by the following correlation (Eq. (1)):

$$\gamma_{ads} \approx \frac{n(\Delta E_{ads} - \mu)}{A} \quad (1)$$

Where n is the number of NTC molecules adsorbed on the Fe surface with an area, A.

Fig. 8 shows the relationship between γ_{ads} and μ at varying coverage levels. The coverage at which γ_{ads} is most negative is considered to be the most stable. It is evident from Fig. 8 that the highest coverage (4/48) is most stable at $\mu > \sim -4.15$ eV.

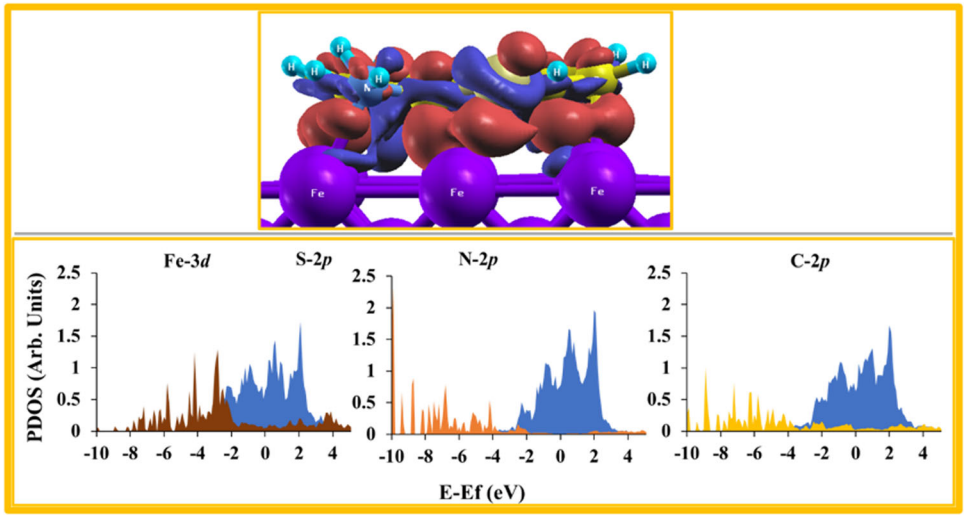

Fig. 5 Electron density difference (top panel) and projected density of states (bottom panel) plots for the most stable Fe (001)-NTC adsorption conformation. In the top panel, blue regions indicate electron depletion while reddish-brown regions indicate electron enrichment. Isovalue: ± 0.003 eV Å^−3.

Table 2. Bader charges before and after adsorption of NTC on Fe surface. S, C and N atoms showing the largest change are marked in bold.

Atoms	Initial	Final	Change (Δ)
S	**−0.156**	**−0.349**	**−0.193**
C	**−0.062**	**−0.25**	**−0.188**
C	**−0.038**	**−0.21**	**−0.172**
C	**−0.066**	**−0.231**	**−0.165**
C	**−0.038**	**−0.201**	**−0.163**
C	−0.053	−0.183	−0.129
C	−0.077	−0.205	−0.128
C	0.011	−0.108	−0.12
C	0.156	0.041	−0.115
C	−0.069	−0.176	−0.107
C	−0.003	−0.108	−0.105
C	−0.003	−0.098	−0.095
N	**−0.999**	**−1.076**	**−0.077**
H	0.131	0.11	−0.021
H	0.087	0.076	−0.011
H	0.096	0.091	−0.005
H	0.4	0.396	−0.004
H	0.416	0.416	0
H	0.074	0.075	0
H	0.05	0.06	0.01
H	0.081	0.093	0.012
H	0.061	0.088	0.027

Thus, starting from the computation of quantum chemical descriptors of 9 sulfur containing compounds, followed by detailed adsorption and coverage studies for the best molecule (NTC) on Fe (001) surface, it has taken a total of only around 225 h (<10 days) of computations on a high-performance computer having the following specifications: 2x AMD EPYC 7532 32-Core Processor (64 cores per node), Frequency: 3.2 GHz. This is comparatively much faster (and also cheaper!) than what would have been otherwise required to identify this molecule using conventional empirical approaches. In the next section, we describe the successful experimental validation of this molecule based on simple weight loss and electrochemical studies.

Weight-loss tests

The values of inhibition efficiency (IE) for various concentrations of NTC were calculated using the below formula (Eq. (2)):

$$\mathrm{IE}(\%) = \left[1 - \frac{\text{corrosion rate with inhibitor}}{\text{corrosion rate without inhibitor}}\right] \text{x } 100 \quad (2)$$

An increase in inhibition efficiency could be seen with increasing concentration, as shown in Table 3. In general, the cathodic reaction for steel corrosion in HCl is hydrogen evolution reaction (HER) characterized by bubble formation and evolution. The rapidity of bubble evolution was observed to decrease with increasing concentration, and could not be noticed at all, for 0.2, 0.7, and 1 mM concentration values suggesting very low corrosion rates, as also, indicated in Table 3 and the lack of metallic lustre loss at these concentration values. This is also consistent with our DFT coverage studies which hint towards the formation of a compact layer with very little lateral repulsion between the molecules.

At 60 °C, the steel underwent rapid corrosion; however, in the presence of 1 mM NTC, the corrosion rate dropped to a value almost 2 orders of magnitude lower. The exceptionally high inhibition efficiency values at both room temperature (97.23%) as well as at 60 °C (98.54%) using merely 1 mM concentration, indicate that NTC can be a highly effective inhibitor for steels in acidic media.

Based on the above experimental data, different adsorption isotherms (like Langmuir, Temkin, and Frumkin) were evaluated. It was found that the adsorption of NTC on mild steel follows the Langmuir isotherm (Fig. 9):

$$\frac{C}{\theta} = \frac{1}{K_{ads}} + C \quad (3)$$

where K_{ads} represents the equilibrium constant for adsorption, C and θ (IE/100) represent the inhibitor concentration (mM) and surface coverage respectively.

From the obtained K_{ads} value using the above expression (Eq. (3)), the free energy of adsorption (ΔG_{ads}) was calculated using

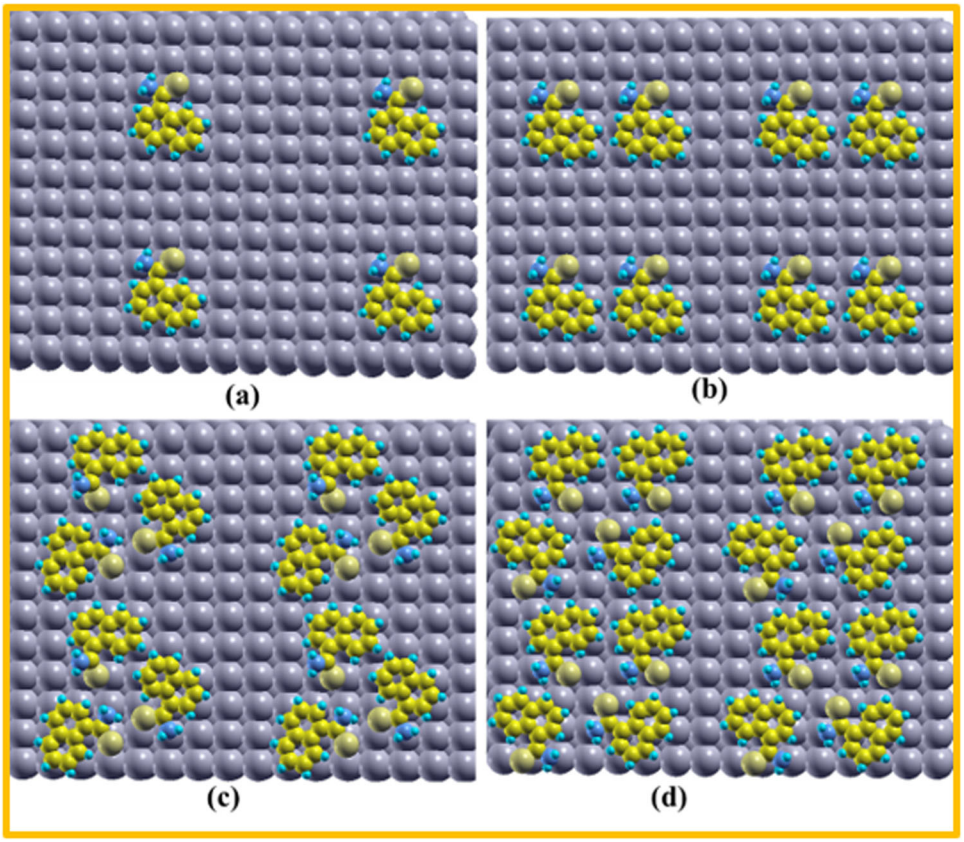

Fig. 6 Optimized structures of NTC on Fe (001) surface at various coverages. a 0.021 (1/48), **b** 0.042 (2/48), **c** 0.062 (3/48), **d** 0.083 (4/48) ML. Legend: Silver, Yellow, Pale Yellow, Blue, and Aqua represent Fe, C, S, N, and H atoms respectively.

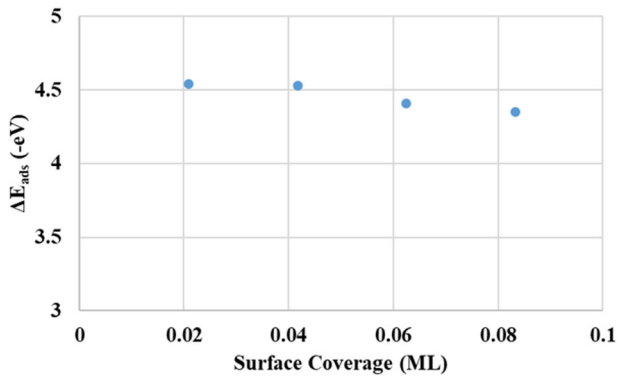

Fig. 7 Variation of ΔE_{ads} (-eV) with surface coverage (ML). Figure shows the influence of surface coverage on adsorption energy of NTC molecule on Fe (001) surface.

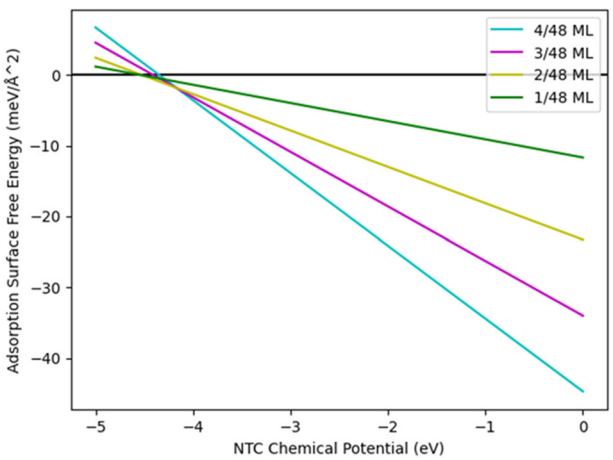

Fig. 8 Adsorption surface free energy (γ_{ads}) versus molecular chemical potential (μ) at different coverages. Coverages studied: 1/48, 2/48, 3/48 and 4/48 ML, where monolayer, ML, is the ratio of the number of NTC molecules to the number of Fe atoms in the first layer of the surface.

the expression (Eq. (4)):

$$\Delta G_{ads} = -RT\ln(55.5K_{ads}) \quad (4)$$

Where, R is the universal gas constant and T is the absolute temperature in Kelvin.

A ΔG_{ads} value of −22.16 kJ mol^−1 was calculated from the above expression. The negative value indicates a spontaneous adsorption of NTC on mild steel. Generally, $\Delta G_{ads} > -20$ kJ mol^−1 (< −40 kJ mol^−1) are considered to indicate physisorption (chemisorption) while intermediate values of $\Delta G_{ads} \in [-20, -40]$ kJ mol^−1 indicate mixed physisorption/chemisorption. Based on the intermediate value of ΔG_{ads} so obtained, it appears that adsorption of NTC on mild steel is via both physical and chemisorption. However, as discussed by Kokalj[23] recently, the value of ΔG_{ads} is not a very reliable criteria to distinguish between physisorption and chemisorption. Instead, he suggests the molecule-surface distance and the electronic structure analysis of the molecule-surface bonding readily available from computational studies as better options. From our DFT computed bond

lengths and electron density difference plots (as reported in the previous sections), it is clear that NTC adsorbs via chemisorption on Fe surface.

Additionally, one of the inherent assumptions in Langmuir adsorption isotherm is that there are no lateral interactions between the adjacent adsorbing molecules. Thus, the heat of adsorption of the corrosion inhibitor ΔH_{ads} is independent of fractional coverage of the inhibitor[24]. Using our DFT computed ΔE_{ads} values as indicators of the experimental ΔH_{ads} values (as reported in earlier section), the small changes in ΔE_{ads} as a function of coverage are validated by the observation of a Langmuir-type adsorption isotherm. It must be mentioned that in our previous publication on *trans*-TCA[20], our DFT computations indicated a Temkin-type isotherm consistent with the experiments.

Table 3. Results of weight-loss experiments.

Conc. (mM)	Temperature (°C)	Corrosion Rate (cm y^−1)	Inhibition Efficiency (%)
Blank	27	1.1081	Not Applicable
0.05	27	0.1073	90.32
0.2	27	0.0674	93.92
0.7	27	0.0645	94.18
1	27	0.0307	97.23
Blank	60	16.4233	Not Applicable
1	60	0.2398	98.54

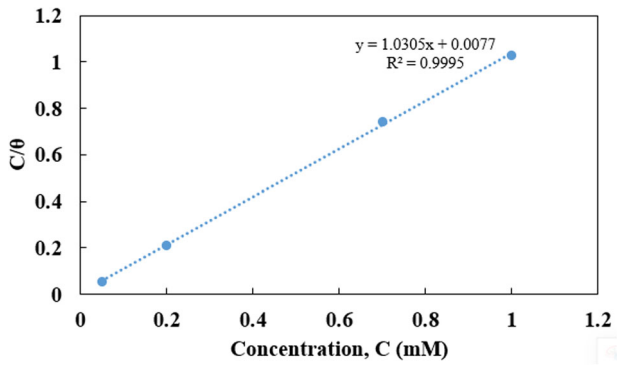

Fig. 9 Langmuir adsorption isotherm plot for NTC adsorption on mild steel in 1 M HCl. Here *C* indicates the concentration of NTC in mM and θ represents surface coverage (IE/100).

Potentiodynamic polarization

NTC seems to be a mixed inhibitor for the current system, as can be deduced from Fig. 10. The polarization plots were analyzed using VersaStudio software to arrive at corrosion current densities (I_{corr}) which are directly proportional to corrosion rates. Table 4 confirms the excellent inhibition efficiencies at all the concentrations tested, in agreement with the weight loss results reported in the previous section. The following equation (Eq. (5)) was employed to calculate the IE's at various concentrations:

$$IE(\%) = \left[1 - \frac{I_{corr}\text{with inhibitor}}{I_{corr}\text{without inhibitor}}\right] x\,100 \quad (5)$$

The polarization resistance was calculated using the Stern-Geary equation (Eq. (6)):

$$R_p = \frac{\beta_c \cdot \beta_a}{2.303 \cdot I_{corr} \cdot (\beta_c + \beta_a)} \quad (6)$$

where, β_a and β_c correspond to the anodic and cathodic slopes in the polarization curve for a particular NTC concentration.

The corrosion current densities show a decrease of corrosion by at least twenty times in 1 M HCl due to the molecule. It is remarkable that the current density at 1 mM NTC (2.93 μA cm^−2)

Table 4. Results of potentiodynamic polarization experiments.

Conc. (mM)	E_{corr} (mV)	I_{corr} (μA cm^−2)	β_c (mV dec^−1)	β_a (mV dec^−1)	R_p (Ω cm^2)	IE (%)
Blank	−427.28	1788.00	150.48	179.88	19.90	-
0.05	−418.11	64.21	109.19	89.83	333.28	96.41
0.20	−436.22	30.71	97.19	97.19	687.12	98.28
0.70	−441.29	7.50	144.84	181.18	4660.23	99.58
1.00	−386.17	2.93	163.38	106.62	9561.29	99.84

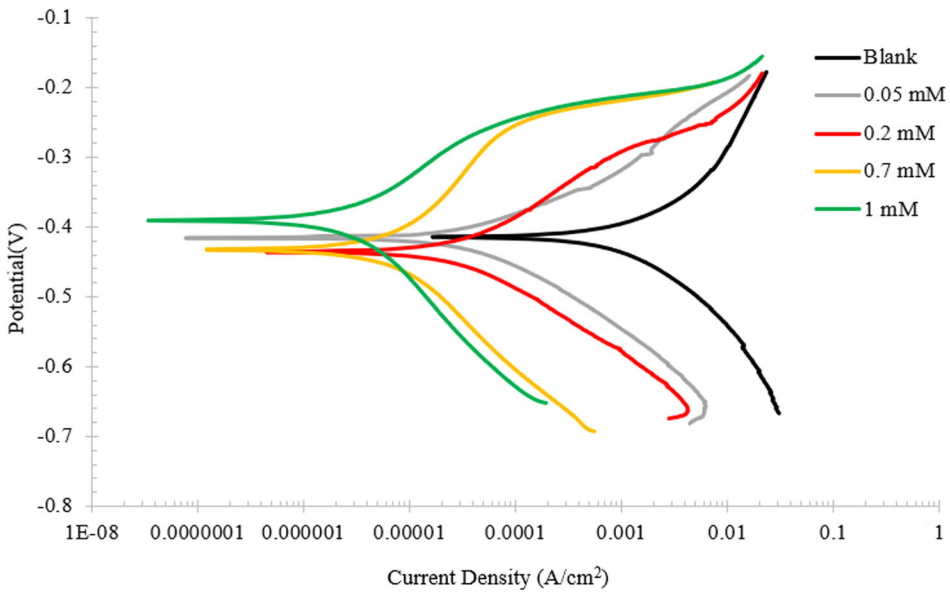

Fig. 10 Polarization curves. Change in current density (A cm^-2) in response to applied potential (V) at various NTC concentrations.

is almost one-fourth of that for the industrially used inhibitor, TCA at 7.5 mM (1000 ppm) for the same steel as reported in our previous publication[16]. This again reinforces our weight-loss results' inference that NTC can be a promising inhibitor for steels in acidic media. Cathodic branches clearly show similarity in behaviour at lower concentrations, which is different from the behaviour at higher concentrations indicating an influence of molecule on the HER beyond 0.2 mM concentration. The anodic branches at three higher concentrations (0.2, 0.7, and 1 mM) differ from that of the lowest concentration (0.05 mM) indicating a change in inhibition mechanism.

Electrochemical impedance spectroscopy

The impedance studies with the molecule at different concentrations resulted in Nyquist plots as shown in Fig. 11, which are analyzed using the ZSimpWin software to understand the influence of the molecule at the metal-solution interface. The behavior of the interface for blank and with various concentrations of inhibitor could be understood using the equivalent electrical circuits R(QR) and R(Q(R(QR))). The IE's at various concentrations of the molecule were calculated using the charge transfer resistance, R_{ct}, with the help of the below equation (Eq. (7)):

$$IE(\%) = \left[1 - \frac{R_{ct}\text{without inhibitor}}{R_{ct}\text{with inhibitor}}\right] x\,100 \quad (7)$$

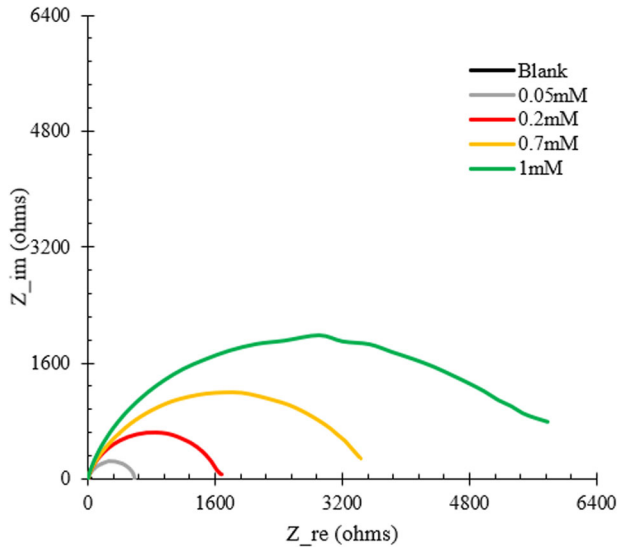

Fig. 11 Nyquist plot showing the impedance response of mild steel in various concentrations of NTC. The increase in diameter of the semi-circle shows increased charge transfer resistance and thereby increased corrosion inhibition with NTC concentration.

The impedance due to constant phase element, Q was evaluated using the equation[25] (Eq. (8)):

$$Z_Q = \frac{1}{Y_o(j\omega)^n} \quad (8)$$

The increasing R_{ct} values suggest an increasing inhibition with concentration (Table 5). A very high R_{ct} (6187 Ω cm^2) as seen with 1 mM implies outstanding protection, thus further supporting the observations from weight-loss and polarization studies.

To summarize, in this paper we highlight the use of first principles density functional theory (DFT) based approaches in order to expedite rational CI design and discovery (and thus, complement experiments). Specifically, our work elucidates the DFT-based discovery of naphthalene 1-thiocarboxamide (NTC) as an excellent CI for steels at both room as well as elevated temperatures (60 °C) in HCl environment. The computed quantum chemical descriptors gave preliminary indication of the promising adsorption ability of NTC. This was further validated with explicit adsorption studies which reveal strong flat chemisorption of NTC onto the Fe (001) surface, forming covalent bonds Fe- S/C/N, further corroborated by EDD and PDOS analyses. Coverage studies also suggest that NTC forms a compact monolayer (essential for good corrosion inhibition) on Fe surface with little lateral repulsions between the adjacent molecules. Gravimetric, potentiodynamic polarization, and Electrochemical Impedance Spectroscopy studies, all confirmed NTC as a remarkable inhibitor for mild steel, thus, testifying the powerful role of DFT in screening & design of new, more efficient corrosion inhibitors.

METHODS

Computational methodologies

Molecular structure of NTC was created in Avogadro −1.2.0[26] and subsequently optimized using NWchem −6.8[27]. For the geometry optimization, the exchange-correlation functional and basis set used were B3LYP[28] and 6-311 + + G**[29], respectively. Energy and force cutoffs of 0.0027 meV and 0.027 meV Å^−1 respectively were used during the optimization. The NTC molecule (Fig. 12) was fully relaxed without any constraints.

The adsorption and coverage studies for NTC on Fe (001) surface were investigated using Plane-Wave, spin-polarized DFT method as implemented in the PWscf code of Quantum Espresso −6.7[30]. The exchange-correlation functional was described using the Perdew-Burke-Ernzerhof (PBE)[31] scheme within the framework of the generalized gradient approximation (GGA). All calculations were performed with a kinetic energy cut-off of 35 Ry and a charge density cut-off of 300 Ry. The van der Waals interactions were taken into account by using Grimme's semi-empirical correlation (DFT-D3)[32] as built in the PWscf code. The bulk Fe was fully optimized using a uniform Monkhorst-Pack k-points mesh[33] of 8x8x8. A 5 × 4 supercell containing 5 layers of Fe-atoms was created, and then fully relaxed until the force on each atom dropped below 0.0025 eV Å^−1. For the surface coverage studies, a larger supercell size of 6 × 8 was employed to accommodate larger number of molecules (1/48, 2/48, 3/48, 4/48 ML). Due to the large system sizes, the surface relaxations and subsequent NTC

Table 5. EIS results for various concentrations of the inhibitor.

Conc. (mM)	R_s (Ω cm^2)	Q-Y_0 ($x10^{-4}$) ((S-sec)^n cm^2)	Q-n	R_{ct} (Ω cm^2)	Q_f-Y_0 ($x10^{-4}$) ((S-sec)^n cm^2)	Q_f-n	R_f (Ω cm^2)	IE (%)
Blank	3.563	13.98	0.896	22.33	—	—	—	—
0.05	3.678	0.902	0.846	597.5	—	—	—	96.26
0.20	3.627	0.3233	0.675	1327	0.2206	0.709	343.3	98.32
0.70	3.315	0.3739	0.628	3000	0.1433	0.896	58.67	99.26
1.00	3.458	0.2668	0.514	6187	0.1	0.908	47.73	99.64

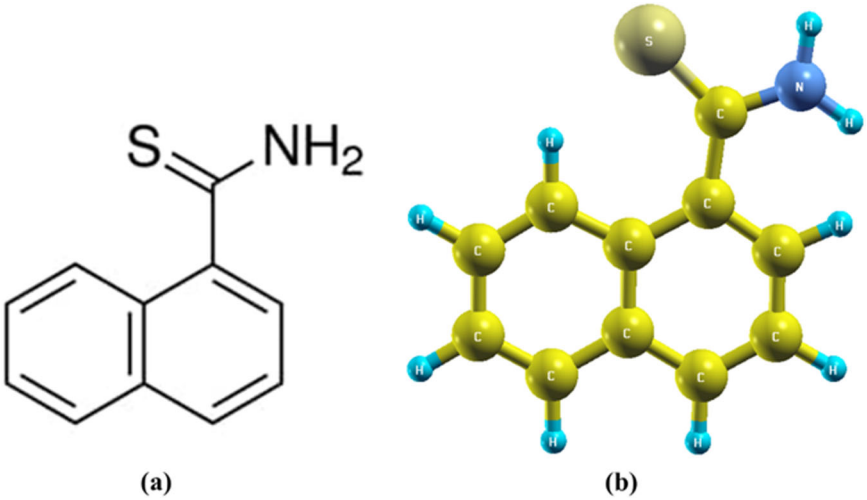

Fig. 12 Molecular structure of NTC. a Chemical structure and **b** DFT optimized molecular geometry of NTC molecule. Legend: Yellow, Pale Yellow, Blue, and Aqua represent C, S, N, and H atoms respectively.

Table 6. Composition of IS2062 mild steel used for experimental study.

Element	C	Si	Mn	P	S	Cr	Mo	Ni	Cu	V	Fe
Wt%	0.044	0.04	1.15	0.028	0.025	0.051	0.001	0.001	0.052	0.011	Bal.

adsorption on Fe surface were carried out at Γ-point. Further details on this section can be found in Kumar et al.[17]. The adsorption energies (ΔE_{ads}) were computed using the expression (Eq. (9)):

$$\Delta E_{ads} = \frac{1}{N}[E_{complex} - (E_{slab} + N * E_{mol})] \quad (9)$$

where, $E_{complex}$, E_{slab}, and E_{mol} are the total energies of the NTC-Fe (001) complex, Fe (001) slab and the NTC molecule respectively, while *N* represents the number of NTC molecules.

Experimental studies

NTC was evaluated for its acid corrosion inhibition characteristics on mild steel using weight-loss tests, potentiodynamic polarization and electrochemical impedance spectroscopy (EIS) in 1 M HCl. The electrochemical tests were carried out at ambient atmospheres i.e. ~27 °C, on 1 cm^2 area of mild steel in 300 ml electrolyte with the help of Ametek K0235 flat cell comprising Pt mesh counter electrode, Ag/AgCl with Vycorr® tip as reference electrode. Ametek PARSTAT 1000 AC/DC Potentiostat was used for electrochemical tests.

Materials

NTC (>97%, CAS: 20300-10-1), Sigma-Aldrich—make was used in all the tests as received. The molecule was evaluated on the coupons of mild steel grade IS2062 with a composition shown in Table 6. Surfaces of metal coupons were prepared on emery papers of grits 80, 150, 240, 400, and 600, following which the coupons were cleaned with acetone and preserved in a desiccator to avoid contact with moisture and/or any corrosion. Tetrahydrofuran was used as a solvent for the molecule.

Weight-loss tests

NTC was tested at various concentrations such as 0.05, 0.2, 0.7, and 1 mM on metal coupons in 1 M HCl under room temperature conditions i.e. ~27 °C. In addition, similar tests were conducted at 60 °C for 1 mM concentration. The coupons were washed with distilled water, followed by air drying, after 2 h of immersion in test solution. The weight-loss was calculated from the observed weights of the coupons before and after the tests.

Potentiodynamic polarization studies

A scan rate of 1 mV s^−1 was used for potentiodynamic polarization studies to increase the potential from −250 mV to +250 mV with respect to Open Circuit Potential (OCP). The results were analysed using VersaStudio, a proprietary software provided by Ametek Scientific Instruments.

Electrochemical impedance spectroscopy

A perturbation voltage of 10 mV was used for impedance studies between the frequencies 10^5 and 10^{-1} Hz of AC signal. The results were analysed using ZSimpWin, a proprietary software provided by Ametek Scientific Instruments.

DATA AVAILABILITY

The datasets used and/or analysed during the current study are available from the corresponding author on reasonable request.

CODE AVAILABILITY

The underlying code for this study [and training/validation datasets] is not publicly available but may be made available to qualified researchers on reasonable request from the corresponding author.

Received: 12 September 2023; Accepted: 25 December 2023;
Published online: 08 January 2024

REFERENCES

1. Chiter, F., Costa, D., Maurice, V. & Marcus, P. Corrosion inhibition at emergent grain boundaries studied by DFT for 2-mercaptobenzothiazole on bi-crystalline copper. *NPJ Mater. Degrad.* **7**, (2023).

2. Solomon, M. M., Uzoma, I. E., Olugbuyiro, J. A. O. & Ademosun, O. T. A censorious appraisal of the oil well acidizing corrosion inhibitors. *J. Petrol. Sci. Eng.* **215**, 110711 (2022).
3. Cairns, A. J., Hull, K. L. & Sayed, M. From design to practice: Development of new acid platforms to address upstream oil and gas production challenges. *ACS Symposium Series* **321**, https://doi.org/10.1021/bk-2019-1320.ch001 (2019).
4. Farhadian, A. et al. Exploration of sunflower oil as a renewable biomass source to develop scalable and highly effective corrosion inhibitors in a 15% HCl medium at high temperatures. *ACS Appl. Mater. Interfaces* **13**, 3119–3138 (2021).
5. Solomon, M. M., Umoren, S. A., Obot, I. B., Sorour, A. A. & Gerengi, H. Exploration of dextran for application as corrosion inhibitor for steel in strong acid environment: Effect of molecular weight, modification, and temperature on efficiency. *ACS Appl. Mater. Interfaces* **10**, 28112–28129 (2018).
6. Daniel M. & Xie A. Development of a New Yellow Metal Corrosion Inhibitor. Paper presented at the *CORROSION 2019*, Nashville, Tennessee, USA, (2019). https://onepetro.org/NACECORR/proceedings-abstract/CORR19/All-CORR19/NACE-2019-12770/127139.
7. Hughes, A. et al. Corrosion inhibition, inhibitor environments, and the role of machine learning. *Corros. Mater. Degrad.* **3**, 672–693 (2022).
8. Winkler, D. Predicting the performance of organic corrosion inhibitors. *Metals* **7**, 553 (2017).
9. Winkler, D. A. et al. Using high throughput experimental data and in silico models to discover alternatives to toxic chromate corrosion inhibitors. *Corros. Sci.* **106**, 229–235 (2016).
10. Winkler, D. A. et al. Towards chromate-free corrosion inhibitors: structure–property models for organic alternatives. *Green. Chem.* **16**, 3349–3357 (2014).
11. Al-Azawi, K. F. et al. Synthesis, inhibition effects and quantum chemical studies of a novel coumarin derivative on the corrosion of mild steel in a hydrochloric acid solution. *Chem. Cent. J.* **10**, 23 (2016).
12. Han, P. et al. Study on synergistic mechanism of inhibitor mixture based on electron transfer behavior. *Sci. Rep.* **6**, 33252 (2016).
13. Huang, Y., Rong, C., Zhang, R. & Liu, S. Evaluating frontier orbital energy and HOMO/LUMO gap with descriptors from density functional reactivity theory. *J. Mol. Model.* **23**, 3 (2016).
14. Nesic, S. et al. Methods for inhibiting metal corrosion, 2017. Patent No. US20170233637A1.
15. Kokalj, A. Is the analysis of molecular electronic structure of corrosion inhibitors sufficient to predict the trend of their inhibition performance? *Electrochim. Acta* **56**, 745–755 (2010).
16. Kumar, D., K, V. M., Jain, V. & Rai, B. Integrating experiments, DFT and characterization for comprehensive corrosion inhibition studies – a case for cinnamaldehyde as an excellent green inhibitor for steels in acidic media. *Corros. Sci.* **208**, 110623 (2022).
17. Kumar, D., Jain, V. & Rai, B. Unravelling the mechanisms of corrosion inhibition of iron by henna extract: A density functional theory study. *Corros. Sci.* **142**, 102–109 (2018).
18. Kovačević, N. & Kokalj, A. Chemistry of the interaction between azole type corrosion inhibitor molecules and metal surfaces. *Mater. Chem. Phys.* **137**, 331–339 (2012).
19. Tang, W., Sanville, E. & Henkelman, G. A grid-based Bader analysis algorithm without lattice bias. *J. Phys.: Condens. Matter* **21**, 084204 (2009).
20. Chiter, F., Costa, D., Pébère, N., Marcus, P. & Lacaze-Dufaure, C. Insight at the atomic scale of Corrosion Inhibition: DFT Study of 8-hydroxyquinoline on oxidized aluminum surfaces. *Phys. Chem. Chem. Phys.* **25**, 4284–4296 (2023).
21. Taylor, C. D., Chandra, A., Vera, J. & Sridhar, N. Multiphysics modelling, quantum chemistry and risk analysis for corrosion inhibitor design and lifetime prediction. *Faraday Discuss.* **180**, 459–477 (2015).
22. Kokalj, A. Comment on the A.B. Rocha's reply to second comment on the paper "on the nature of inhibition performance of imidazole on iron surface". *Corros. Sci.* **79**, 215–220 (2014).
23. Kokalj, A. Corrosion inhibitors: physisorbed or chemisorbed? *Corr. Sci.* **196**, 109939 (2022).
24. McCafferty, E. Introduction to Corrosion Science, 1st edn. p. 376 (Springer, 2010) .
25. Orazem, M. E. & Tribollet, B. Electrochemical impedance spectroscopy. 383–389 (John Wiley & Sons, 2008).
26. Hanwell, M. D. et al. Avogadro: an advanced semantic chemical editor, visualization, and Analysis Platform. *J. Cheminf.* **4**, 17 (2012).
27. Valiev, M. et al. NWChem: a comprehensive and scalable open-source solution for large scale molecular simulations. *Comput. Phys. Commun.* **181**, 1477–1489 (2010).
28. Lee, C., Yang, W. & Parr, R. G. Development of the colle-salvetti correlation-energy formula into a functional of the electron density. *Phys. Rev. B* **37**, 785–789 (1988).
29. Ditchfield, R., Hehre, W. J. & Pople, J. A. Self-consistent molecular-orbital methods. ix. an extended gaussian-type basis for molecular-orbital studies of organic molecules. *J. Chem. Phys.* **54**, 724–728 (1971).
30. Giannozzi, P. et al. Quantum Espresso: A modular and open-source software project for quantum simulations of materials. *J. Phys.: Condens. Matter* **21**, 395502 (2009).
31. Perdew, J. P., Burke, K. & Ernzerhof, M. Generalized gradient approximation made simple. *Phys. Rev. Lett.* **77**, 3865–3868 (1996).
32. Grimme, S., Antony, J., Ehrlich, S. & Krieg, H. A consistent and accurate ab initio parametrization of density functional dispersion correction (DFT-D) for the 94 elements H-pu. *J. Chem. Phys.* **132**, 154104 (2010).
33. Monkhorst, H. J. & Pack, J. D. Special points for Brillouin-zone integrations. *Phys. Rev. B* **13**, 5188–5192 (1976).

ACKNOWLEDGEMENTS

We thank Mr. K. Ananth Krishnan – Ex-Chief Technology Officer at Tata Consultancy Services (TCS), for the funding and encouragement towards this research.

AUTHOR CONTRIBUTIONS

Detailed DFT studies were conducted by D.K. to identify the corrosion inhibitor under consideration. Experiments were carried out by V.K., while V.J. provided guidance throughout the project execution. The manuscript preparation saw equal contributions from D.K., V.K., and V.J. The project was supervised by B.R. The final manuscript was read and approved by all authors.

COMPETING INTERESTS

The authors declare no competing interests.

ADDITIONAL INFORMATION

Correspondence and requests for materials should be addressed to Dharmendr Kumar.

Reprints and permission information is available at http://www.nature.com/reprints

Publisher's note Springer Nature remains neutral with regard to jurisdictional claims in published maps and institutional affiliations.